Article

Cell Reports

Structure Guided Design of Potent and Selective Ponatinib-Based Hybrid Inhibitors for RIPK1

Graphical Abstract

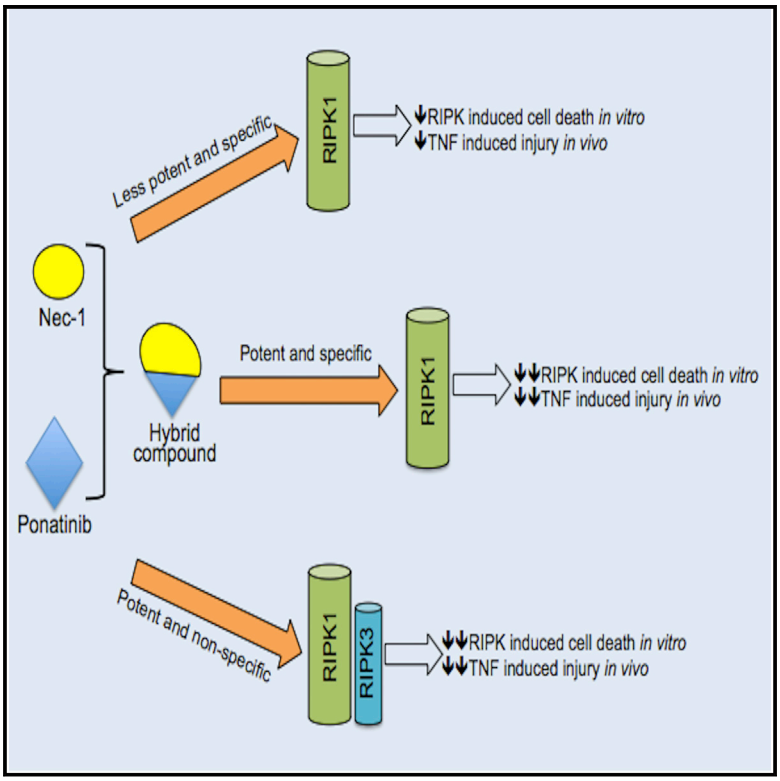

Highlights

- Ponatinib is identified as a dual RIPK1 and RIPK3 inhibitor in vitro
- Ponatinib analogs, selective for RIPK1 versus Abl and RIPK2/3, are described
- Selective and potent ponatinib-Nec-1 (PN) hybrids are developed to target RIPK1
- These molecules are efficient inhibitors of TNF-α-driven pathology in vivo

Authors

Malek Najjar, Chalada Suebsuwong, ..., Gregory D. Cuny, Alexei Degterev

Correspondence

alexei.degterev@tufts.edu

In Brief

Najjar et al. find that the Bcr-Abl inhibitor ponatinib is also a dual RIPK1 and RIPK3 inhibitor with cytoprotective properties in RIPK1- and RIPK3-driven cell death, both in vitro and during inflammatory pathology in vivo. The authors further outline strategies to generate ponatinib-based selective RIPK1 inhibitors.

Najjar et al., 2015, Cell Reports *10*, 1850–1860
March 24, 2015 ©2015 The Authors
http://dx.doi.org/10.1016/j.celrep.2015.02.052

OPEN ACCESS
CellPress

Cell Reports
Article

Structure Guided Design of Potent and Selective Ponatinib-Based Hybrid Inhibitors for RIPK1

Malek Najjar,[1,9] Chalada Suebsuwong,[3,9] Soumya S. Ray,[5,9] Roshan J. Thapa,[6] Jenny L. Maki,[2] Shoko Nogusa,[6] Saumil Shah,[2] Danish Saleh,[2] Peter J. Gough,[7] John Bertin,[7] Junying Yuan,[8] Siddharth Balachandran,[6] Gregory D. Cuny,[4] and Alexei Degterev[1,2,*]

[1]Department of Integrative Physiology and Pathobiology, Graduate Program in Pharmacology and Experimental Therapeutics, Sackler School of Graduate Biomedical Sciences, Tufts University School of Medicine, Boston, MA 02111, USA
[2]Department of Developmental, Molecular & Chemical Biology, Tufts University School of Medicine, Boston, MA 02111, USA
[3]Department of Chemistry, University of Houston, Houston, TX 77204, USA
[4]Department of Pharmacological and Pharmaceutical Sciences, College of Pharmacy, University of Houston, Houston, TX 77204, USA
[5]Center for Neurologic Diseases, Department of Neurology, Brigham & Women's Hospital and Harvard Medical School, Cambridge, MA 02139, USA
[6]Immune Cell Development and Host Defense Program, Fox Chase Cancer Center, 333 Cottman Avenue, Philadelphia, PA 19111, USA
[7]Pattern Recognition Receptor Discovery Performance Unit, Immuno-Inflammation Therapeutic Area, GlaxoSmithKline, Collegeville, PA 19426, USA
[8]Department of Cell Biology, Harvard Medical School, Boston, MA 02115, USA
[9]Co-first author
*Correspondence: alexei.degterev@tufts.edu
http://dx.doi.org/10.1016/j.celrep.2015.02.052

SUMMARY

RIPK1 and RIPK3, two closely related RIPK family members, have emerged as important regulators of pathologic cell death and inflammation. In the current work, we report that the Bcr-Abl inhibitor and anti-leukemia agent ponatinib is also a first-in-class dual inhibitor of RIPK1 and RIPK3. Ponatinib potently inhibited multiple paradigms of RIPK1- and RIPK3-dependent cell death and inflammatory tumor necrosis factor alpha (TNF-α) gene transcription. We further describe design strategies that utilize the ponatinib scaffold to develop two classes of inhibitors (CS and PN series), each with greatly improved selectivity for RIPK1. In particular, we detail the development of PN10, a highly potent and selective "hybrid" RIPK1 inhibitor, capturing the best properties of two different allosteric RIPK1 inhibitors, ponatinib and necrostatin-1. Finally, we show that RIPK1 inhibitors from both classes are powerful blockers of TNF-induced injury in vivo. Altogether, these findings outline promising candidate molecules and design approaches for targeting RIPK1- and RIPK3-driven inflammatory pathologies.

INTRODUCTION

Receptor interacting protein kinases (RIPKs) are a family of Ser/Thr and Tyr kinases with important roles in inflammation and innate immunity. The kinase activities of RIPK1 and RIPK3 were found to be critical for the activation of necroptotic cell death pathway by multiple stimuli, including tumor necrosis factor alpha (TNF-α) family of cytokines, interferons (IFNs), and Toll-like receptor (TLR) ligands (Christofferson and Yuan, 2010; Vanlangenakker et al., 2012). Importantly, RIPK1 and RIPK3 kinases have been implicated in a variety of pathologic settings that currently lack effective therapies, including stroke, myocardial infarction, retinal injuries, lethal systemic inflammatory response syndrome (SIRS) and chronic gut and skin inflammation, and acute pancreatitis (Linkermann and Green, 2014).

We have previously described the development of necrostatins, a class of efficient small molecule inhibitors of necroptosis (Figure 1A) (Degterev et al., 2005, 2008). Importantly, an optimized analog of necrostatin-1, 7-Cl-O-Nec-1 (used throughout this paper and referred to as Nec-1), displayed unusually exclusive selectivity toward RIPK1 kinase and lacked necroptosis inhibitory activity in the absence of RIPK1 (Christofferson et al., 2012; Dillon et al., 2014). Structurally, this inhibitor, as well as other necrostatins, was found to stabilize an unusual inactive αC-Glu-out/DLG-out conformation of RIPK1 characterized by the large movement of the αC helix (αC-out) from the active state in conjunction with the inactive conformation of the DLG motif (Figure 1B) (Xie et al., 2013). DFG (Asp-Phe-Gly) (or DLG in a subset of kinases, like RIPK1) is a highly conserved tripeptide motif present in most human kinases, which changes from the inactive "DXG-out" conformation to the active "DXG-in" state, where Asp is aligned with other residues in the active center and is involved in Mg^{2+} binding. In addition, Nec-1 was found to interact exclusively with the DLG-out "back" pocket of RIPK1 without contacts in the more redundant ATP binding site, likely explaining its unusually high degree of selectivity. On the other hand, extensive structure-activity relationship (SAR) analysis of Nec-1 and other necrostatins revealed that even small changes to these molecules led to the robust loss of activity and failed to identify clear directions to significantly increase affinity of these moderately potent (e.g., cellular IC_{50} of 7Cl-O-Nec-1 = 210 nM)

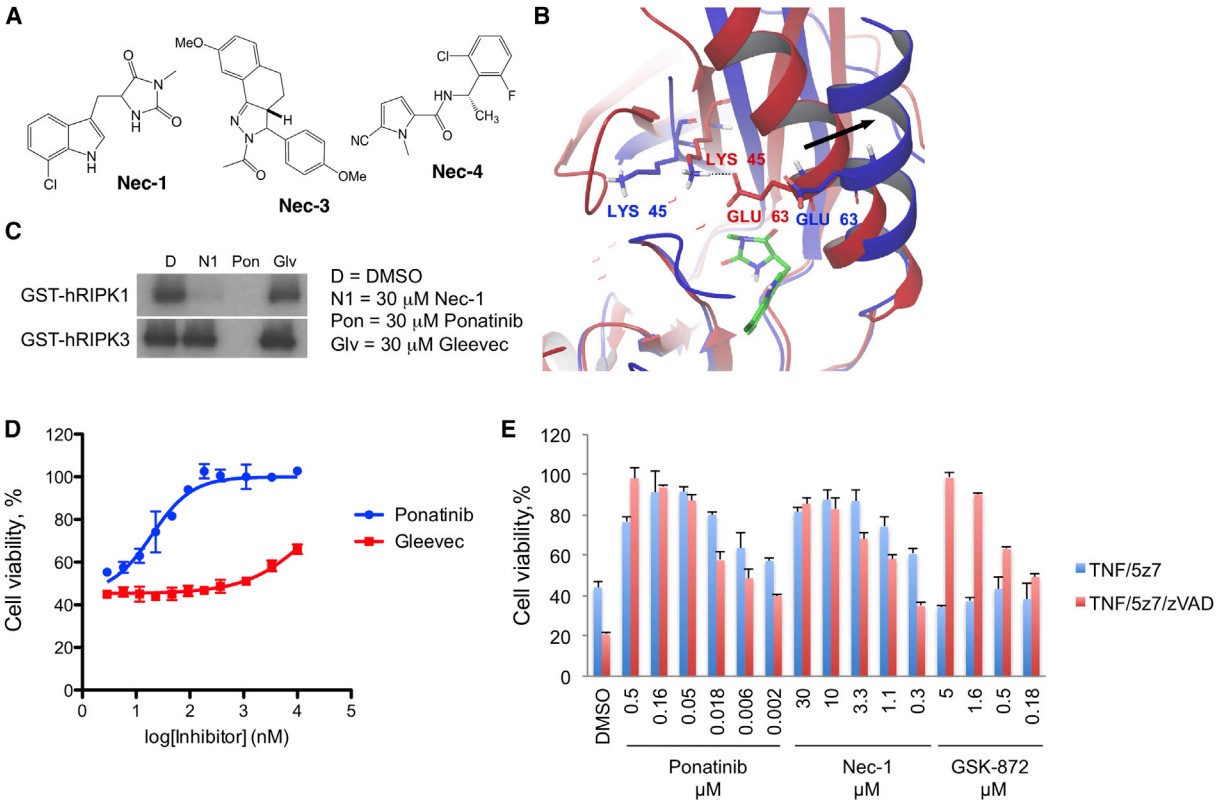

Figure 1. Inhibition of Necroptosis and RIPK1 Kinase by Ponatinib

(A) Structures of necrostatins.

(B) Comparison of Glu-in/DLG-out (red, PDB: 4NEU) and Glu-out/DLG-out (blue, PDB: 4ITH) conformations of RIPK1 kinase reveals movement of αC helix. Movement of αC helix is indicated by black arrow. Position of Nec-1 in Glu-out/DLG-out structure is shown (Nec-1, green). Ionic bond between Glu63 and Lys45 in Glu-in conformation is indicated.

(C) Ponatinib inhibits recombinant RIPK1 and RIPK3 kinases in vitro. Two-μM kinases were used in the in vitro ^{32}P autophosphorylation assay. Nec-1 only inhibited RIPK1, while Gleevec lacked activity against both kinases.

(D) Gleevec does not inhibit necroptosis. FADD-deficient Jurkat cells were treated with 10-ng/ml human TNF-α in the presence of 11 point dose ranges of Ponatinib and Gleevec for 24 hr.

(E) Ponatinib inhibits TNF-induced cell death in the presence of 100-nM TAK1 inhibitor 5z-7-oxozeaenol. MEFs were stimulated with 10-ng/ml mouse TNF-α with 5z-7 for 24 hr to induce RIPK1-dependent apoptosis. To induce RIPK3-dependent necroptosis, cells were additionally treated with 50-μM zVAD.fmk. Inhibition of cell death by indicated concentrations of ponatinib, Nec-1, and RIPK3 inhibitor GSK-872 was determined. Cell viability data are presented as mean ± SD.

See also Figure S1.

molecules (Choi et al., 2012; Jagtap et al., 2007; Teng et al., 2005, 2007, 2008). Furthermore, necrostatins could have physical limitations on maximal robustness due to the small size of the molecules and an energy penalty due to the loss of a strong Glu/Lys interaction in αC-Glu-out conformation (Figure 1B). These shortcomings prompted us to explore additional ways to target RIPK1 that would capture the excellent selectivity of necrostatins while achieving significant increases in activity.

RESULTS

Discovery of Ponatinib as the First-in-Class Dual Inhibitor of RIPK1 and RIPK3

We observed that Glu-in/DLG-out conformation of RIPK1 closely resembles that of Abl (Zhou et al., 2011) (Figure S1A). Based on this similarity, we screened small panel type 2 tyrosine kinase inhibitors, many of which display potent activity against Abl kinase. The screen identified two molecules, ponatinib and DCC-2036, that efficiently attenuated necroptosis (Figure S1B). Subsequent in vitro experiments showed that both ponatinib and DCC-2036 inhibited not only RIPK1, but also RIPK3 and another member of RIPK family RIPK2 (Canning et al., personal communication), identifying them as the first reported pan-RIPK1/RIPK2/ RIPK3 inhibitors (Table 1). Both molecules efficiently inhibited RIPK1- and RIPK3-dependent necroptosis in TNFα-stimulated FADD-deficient Jurkat cells with activity of ponatinib exceeding that of Nec-1 (Figure S1B; Table 1). DCC-2036 displayed much poorer (>10-fold lower) cellular activity than ponatinib. We confirmed the in vitro activity of ponatinib by showing inhibition of RIPK1 and RIPK3 in a ^{32}P autophosphorylation assay (Degterev et al., 2008) (Figure 1C) and of RIPK1 in an HTRF assay (Maki and Degterev, 2013) (Figure S1C). As a negative control,

Table 1. Inhibition of RIPKs and Necroptosis by Ponatinib and DCC-2036

Compound	IC_{50}, nM ADPGlo, RIPK2	IC_{50}, nM ADPGlo, RIPK3	IC_{50}, nM ADPGlo, RIPK1	IC_{50}, nM Jurkat Cell Necroptosis Assay (RIPK1- and RIPK3-Dependent)
Ponatinib	14[a]	1.6	12	34
DCC-2036	520	18	5.7	373
Nec-1	NI	NI	760	210

In vitro kinase assays were performed with recombinant RIPK2 (10 ng), RIPK1, and RIPK3 (20 ng) kinases using ADP-Glo assay (Promega). For necroptosis assay, human FADD-deficient Jurkat cells were stimulated with 10-ng/ml human TNF-α for 24 hr. In all cases, activity of compounds was determined using 8-point (HEK cells), 10-point (kinases), or 11-point (necroptosis) dose response series in duplicate. Curve fitting to calculate IC_{50} values was performed using GraphPad software. NI, no inhibition up to 10 μM (maximal concentration in assays).
[a]Canning et al., personal communication.

a different Abl inhibitor, Gleevec (Imatinib), neither inhibited RIPK1 and RIPK3 kinases in vitro (Figure 1C) nor prevented necroptosis (Figure 1D).

Ponatinib was also effective in other paradigms of RIPK-driven cell death besides TNF-α-induced necroptosis. Ponatinib afforded potent (IC_{50} = 7 nM) protection of immortalized mouse macrophages (iBMMs), undergoing TLR4-induced necroptosis (He et al., 2011) in response to lipopolysaccharide (LPS) and the pan-caspase inhibitor zVAD.fmk (Figure S1D). It also protected mouse embryonic fibroblasts (MEFs) stimulated with TNF-α in the presence of the TAK1 inhibitor 5z-7-oxozeaenol (5z-7), a combination previously reported to induce RIPK1-dependent but RIPK3-independent apoptosis, rather than necroptosis (Figure 1E) (Dondelinger et al., 2013). Notably, in both cases, ponatinib displayed higher activity than Nec-1 and higher and broader activity than RIPK3 inhibitor GSK-872 (Kaiser et al., 2013), which did not inhibit RIPK1-dependent apoptosis (Figure 1E).

Identification of RIPK1 Kinase-Selective Analogs of Ponatinib

Despite excellent activity against RIPK1 and RIPK3 kinases, ponatinib's relative lack of specificity limits its utility as a probe to dissect RIPK1- and RIPK3-dependent signaling events and raises concerns over the safety of its use as a cytoprotective agent in clinical settings. Thus, we explored strategies to make ponatinib more selective by retaining elements of its scaffold that confer high affinity toward RIPKs, while introducing modifications enhancing selectivity toward RIPK1 and/or RIPK3. We generated a docked model of RIPK1/ponatinib based on the recently described co-crystal structure of ponatinib with a homologous kinase RIPK2 (PDB 4C8B; Canning et al., personal communication), which revealed potential differences in the binding pocket of RIPK1 versus RIPK2/Abl around the central phenyl ring of ponatinib (Ring A; Figure S2). Namely, RIPK1 contains a smaller hydrophobic pocket accommodating the methyl of Ring A (Ile43, Lys45, Leu90 and Met92 [gatekeeper]; Figure 2A) compared with Abl, RIPK2, and RIPK3, which contain a smaller hydrophilic Thr gatekeeper, but a bulkier DFG motif (Figure 2B). Notably, the combination of a DLG (rather than DFG) and a medium-size hydrophobic gatekeeper (Met) is unique for RIPK1 based on human kinome alignment (http://kinase.com/human/kinome/phylogeny.html). We next tested whether these differences could be exploited to achieve selectivity between RIPK1 versus Abl/RIPK2/RIPK3. We generated an analog lacking the Ring A methyl group (CS1; Figure 2C), which showed reduced inhibition for all three RIPKs and Abl (Table 2), consistent with this group making positive, but not critical, hydrophobic contacts in the identified lipophilic pocket. Unexpectedly, bulkier substituents in this position (CS2–CS6) displayed an abrupt loss of activity against Abl, RIPK2, and RIPK3 (RIPK3 < RIPK2 < Abl), and the *tert*-butyl (CS6) analog retained activity only against RIPK1 (Table 2). To better understand the selectivity of these analogs, profiling was performed against a panel of 90 WT human kinases using CS analogs, representing a gradual increase in the size of Ring A's substituent. These data (Figure 3A; Table S1) indicated both an increase in selectivity and a general decrease in activity with introduction of bulkier groups on Ring A, which can be expected based on the limited size of the binding pocket. CS6 displayed the highest selectivity against the kinase panel. In particular, it showed no inhibition of RIPK2, ~670-fold lower inhibition of phosphorylated Abl compared with ponatinib, but only ~10-fold reduction in activity against RIPK1 (Figures 3A and 3B; Table S1). Overall, this SAR of ponatinib achieved better RIPK1 selectivity, albeit with modestly reduced activity toward RIPK1.

The selectivity of CS6 for RIPK1 appeared counterintuitive since RIPK1's bulkier gatekeeper residue (Met) makes its pocket more restrictive (compared with Thr of Abl/RIPK2/RIPK3). Notably, the bulky T315I gatekeeper mutant of Abl was inhibited ~60- to 70-fold less by CS5 or CS6 compared with ponatinib (Table S1) and was not inhibited by these molecules in the ADPGlo assay (data not shown), suggesting that differences in gatekeeper size per se do not explain the selectivity of the CS series toward RIPK1. Another possibility is that the bulkier and more rigid Phe of the DFG (in place of Leu157 of RIPK1 DLG; Figure 2B) may prevent induced fit accommodating the Ring A with a substituent exceeding a specific size threshold. To further address this question, we calculated the per-atom energy contribution to binding for ponatinib and CS6 in RIPK1 and Abl using a MM-GBSA approach (Beard et al., 2013; Hayes et al., 2011) with local hierarchal sampling of the residue conformations in the DXG motif, the gatekeeper residue, and the ligand atoms (details in Experimental Procedures) (Figures 3C and S3A). The results indeed indicated that CS6 had an energetically more favorable fit (indicated in blue) in RIPK1 compared with Abl (indicated in red). Furthermore, introduction of Phe residue (L157F and L157F/M92T mutants of RIPK1) rendered CS6 binding to RIPK1 energetically unfavorable (Figure S3A). To experimentally confirm the role of the DLG, we tested the L157F mutant of RIPK1 in a ^{32}P autophosphorylation assay. L157F RIPK1 was

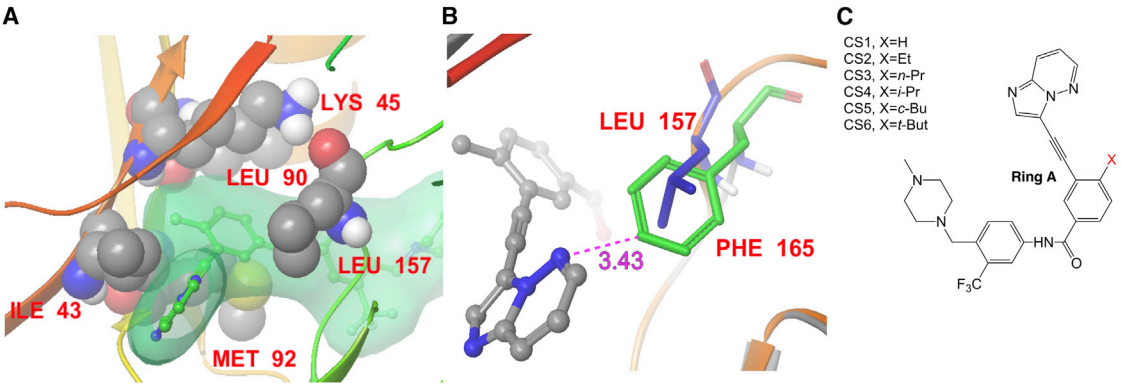

Figure 2. Modeling Interactions of Ponatinib CS Analogs with RIPK1 and RIPK2 Kinases

(A) Ring A of ponatinib inserts into the lipophilic pocket formed by aliphatic portions of side-chains of Ile43, Lys45, Leu90, and Met92. The backside of the molecule is aligned with the side chain of Leu157 of DLG motif.

(B) Alignment of Leu157 of RIPK1 DLG and Phe165 of RIPK2 DFG motifs. Phe165 is in close proximity with the ATP binding pocket moiety of ponatinib.

(C) Chemical structures of CS analogs of ponatinib.

See also Figure S2.

inhibited poorly by all ponatinib analogs (Figure 3D). L157F/M92T RIPK1 containing the "Abl/RIPK2/RIPK3" combination of DFG/Thr gatekeeper was inhibited by ponatinib and CS4, but no longer inhibited by CS6, similar to Abl (Figure 3D; Table 2). Overall, these data suggested that the more flexible DLG allows RIPK1 to accommodate larger substituents attached to the Ring A of ponatinib, while the Met92 gatekeeper restricts the binding pocket, leading to the reduced inhibition of RIPK1 by CS6. These data highlighted that relatively small differences between RIPK1 and other kinases can be exploited to achieve significant gains in selectivity; however, these gains may be limited with respect to the entire kinome.

Inhibition of RIPK3-Dependent Cell Death by Ponatinib

Recent evidence suggest that in a number of situations, such as stimulation with IFNs, TLR3 agonists, and infection with mouse herpes virus lacking endogenous RIP inhibitor (vIRA), necroptosis may bypass RIPK1 and proceed through direct RIPK3 activation (Dillon et al., 2014; Kaiser et al., 2013; Upton et al., 2012). Along these lines, genetic deletion of *RIPK1* in MEF cells was found to promote RIPK3-dependent cell death in response to IFNγ (Dillon et al., 2014; Kaiser et al., 2014). We confirmed that activation of cell death in *RIPK1*$^{-/-}$ MEFs by IFNγ was dependent on RIPK3 by demonstrating blockade of cell death by the RIPK3 inhibitor GSK-872 (Figure S3B). Ponatinib (Figure 3E) efficiently inhibited this form of cell death at ~10-fold lower concentration compared with GSK-872 (Figure S3B). Importantly, inhibition of cell death was greatly reduced with CS4, and very marginal protection was seen with CS6 (Figure 3E), consistent with the loss of RIPK3 kinase inhibition in vitro (Table 2). Neither Gleevec nor Nilotininb, which are potent inhibitors of Abl but do not inhibit RIPK1 or RIPK3 (Figure 1; data not shown), inhibited IFNγ-induced cell death, excluding a role for Abl in this model of cell death (Figure S3C). Ponatinib also displayed activity in a second paradigm of RIPK3-specific cell death induced by TLR3 agonist poly(I:C)/zVAD.fmk (Kaiser et al., 2013) (Figure 3F). CS4 again displayed reduced activity, while CS6 provided only marginal protection on par with that demonstrated by Nec-1. Overall, these data confirmed that ponatinib can inhibit RIPK3 kinase-driven cell death and supported the selectivity of CS analogs for RIPK1 over RIPK3.

Development of Nec-1/Ponatinib "Hybrid" Inhibitors

A comparison of the Glu-in and Glu-out conformations of RIPK1 DLG-out pocket suggested that the latter provides more space for inhibitor binding (Figure S4A) (187 versus 209 Å^3, respectively). The RIPK1•Nec-1 co-crystal structure revealed that Nec-1 assumes a "kinked" conformation (Figure 1B) (Xie et al., 2013) in the DLG-out pocket, allowing multiple specific affinity-driving contacts within the pocket that would be precluded in a more narrow Glu-in conformation as seen in the RIPK1/ponatinib docked model (Figure S4B). In contrast, flat hydrophobic moieties present in typical type 2 inhibitors, like ponatinib (Figure S2), provide a good fit with the narrower Glu-in/DXG-out conformation. Thus, we hypothesized that highly selective Glu-out/DXG-out-targeting groups, such as those present in necrostatins, might provide an excellent complement to the current type 2 inhibitor scaffolds by replacing the less selective DFG pocket binding components of current type 2 inhibitors (Figure 4A), which may allow us to capture both high activity of inhibitors, like ponatinib, and excellent selectivity of necrostatins.

Accordingly, we designed and synthesized a set of ponatinib/necrostatin-1 "hybrid" inhibitors, which we termed the "PN" series. Binding site alignment of ponatinib/RIPK1 (docked model) and Nec-1/RIPK1 (co-crystal structure) revealed that the urea of Nec-1 and the amide of ponatinib both form hydrogen bonds with the backbone of Asp157 of the DLG, providing a convenient point to connect Nec-1 to Ring A of ponatinib (distance ~2.7Å; Figure S4C). We initially designed three PN molecules (PN1-3), which showed good docking scores by GLIDE XP (Friesner et al., 2004). However, these molecules displayed lower activity toward RIPK1 compared with either Nec-1 or ponatinib (Figure 4B). We speculated that the reduced activity might have resulted from suboptimal geometry of the hybrids or from

Table 2. In Vitro and Cellular Activities of Ponatinib CS Analogs, Necrostatins, and PN10

Compound	IC_{50}, nM ADPGlo,Abl	IC_{50}, nM ADPGlo,RIPK2	IC_{50}, nM HEKBlue Cell Assay, (RIPK2-Dependent)	IC_{50}, nM ADPGlo,RIPK3	IC_{50}, nM ADPGlo,RIPK1	IC_{50}, nM Jurkat Cell Necroptosis Assay (RIPK1- and RIPK3-Dependent)
Ponatinib	1.4	14[a]	1.0[a]	1.6	12	34
CS1	6.7	63	3.6	7.4	42	219
CS2	5.1	45	30	49	13	48
CS3	32	1400	617	2700	33	135
CS4	31	630	472	460	19	75
CS5	181.7	5096	NI	NI	28	471
CS6	34000	NI	NI	NI	26	354
Nec-3	NI	NI	NI	NI	840	260
Nec-1	NI	NI	NI	NI	760	210
Nec-4	NI	NI	NI	NI	330	80
PN10	NI	1400	1193	NI	90	10

Experiments were performed as described in Table 1. In addition, in vitro kinase assays were performed with recombinant Abl (1 ng) using ADP-Glo assay. For RIPK2 cellular assay, human HEK cells expressing NOD2 and NFkB-SEAP reporter were stimulated for 8 hr with 1-μg/ml L18-MDP (Invivogen), followed by detection using QUANTI-Blue SEAP reagent (Invivogen). NI, no inhibition up to 10 μM (maximal concentration in assays).
[a]Canning et al., personal communication.

incompatible conformations of the hinge in the Glu-in/DLG-out and Glu-out/DLG-out conformations.

To determine whether the ponatinib portion of PN hybrids made any contribution to RIPK1 binding, we next introduced small changes to this part of the molecule. Resulting hybrids (PN4-6) revealed a sharp SAR for the hinge-binding fragment, suggesting that the ponatinib portion of PNs likely makes contacts in the ATP pocket, but that the geometry of the hybrids still was not optimal. Based on these data, we designed a panel of PNs with a broader range of linkers between the ponatinib and Nec-1 fragments. These molecules were again docked into RIPK1 using GLIDE XP (Figure S4D) with the added constraint that molecules form hydrogen bonds to the backbone amide of Met95 of the hinge and at least two out of the three hydrogen bonds observed for Nec-1 in the DLG-out pocket Val76 (backbone carbonyl), Leu157 (backbone amide), or Ser161 (side-chain alcohol) (Xie et al., 2013) to ensure that the hybrid retains contacts to the hinge and a binding mode for the Nec-1 substructure that is consistent with the crystallographic pose (<0.5 Å). A much smaller subset of inhibitors that produced docking poses satisfying these criteria was again docked without any hydrogen bond constraints (Figure S4D). We used two independent docking calculations to ensure that we selected molecules with the appropriate binding mode and did not bias our selection due to the initial hydrogen bonding constraints. As a result, several molecules assuming a binding pose in both docking experiments, comparable to Nec-1/ponatinib (Figure S4E), and displaying good docking scores (Figure S4F) were synthesized (Figure 4B). PN12, which did not fit these criteria, was included to further characterize the effect of the linker length on activity. Excitingly, one molecule in this set (PN10) displayed excellent in vitro activity against RIPK1, exceeding that of Nec-1 (Table 2). In addition, PN10 showed better activity in necroptosis assays than either Nec-1 (~20-fold) or ponatinib (~3-fold), suggesting that we have indeed achieved a good fit for both the ponatinib and Nec-1 fragments in PN10. Most importantly, PN10 displayed excellent selectivity for RIPK1 in a 90 kinases panel screen (Figures 4D and 4E). In ADPGlo and HEKBlue assays, some inhibition of RIPK2 was observed, but it was greatly reduced compared with ponatinib (Nec-1 lacks activity against RIPK2) (Table 2). Overall, these data suggested that it is possible to take advantage of the unique properties of both Glu-out/DXG-out inhibitors like Nec-1 (selectivity) and Glu-in/DXG-out inhibitors like ponatinib (binding affinity) to develop both potent and highly selective type 2 inhibitors of RIPK1 kinase.

Surprisingly, while PN10 showed improved in vitro and cellular activity against RIPK1 and necroptosis compared with other necrostatins, it was still a ~9-fold weaker inhibitor than ponatinib in vitro, despite ~3-fold better cellular activity (Table 2). This may reflect differences in the binding modes between necrostatins, including PN10, and ponatinib. We noticed that all necrostatins displayed lower activity in an in vitro kinase assay compared to cellular inhibition of necroptosis (~3- to 5-fold better IC_{50} in cells than in vitro) (Table 2). In contrast, ponatinib displayed ~3-fold higher activity in vitro than in cells. We have previously optimized the length of RIPK1's kinase domain (recombinant RIPK1, amino acids 1–327) to maximize its catalytic activity (Maki and Degterev, 2013; Maki et al., 2013) and, hence, the kinase active Glu-in conformation. The Glu-in conformation creates an additional energy barrier (due to the loss of a highly conserved Glu/Lys ionic bond in the Glu-out conformation) that must be overcome by necrostatins (Figure 1B). This is not the case for Glu-in inhibitors like ponatinib, explaining poorer than expected performance of necrostatins in the in vitro kinase assay. Notably, another previously described Glu-out inhibitor, the Abl inhibitor PD166326 (Levinson et al., 2006), was similarly ~20-fold less active in vitro compared with cellular assays (Huron et al., 2003).

A potential steric clash with the bulky gatekeeper presents a major challenge for the design of optimal type 2 inhibitors, as demonstrated by the inability of most type 2 Abl inhibitors to efficiently target the T315I gatekeeper mutant (Zhou et al., 2011).

A

Compound Name	Selectivity Score Type	Number of Hits	Number of Non-Mutant Kinases	Screening Concentration (nM)	Selectivity Score
Pon	S(35)	41	90	1000	0.456
	S(10)	33	90	1000	0.367
	S(1)	24	90	1000	0.267
CS4	S(35)	24	90	1000	0.267
	S(10)	14	90	1000	0.156
	S(1)	5	90	1000	0.056
CS5	S(35)	11	90	1000	0.122
	S(10)	6	90	1000	0.067
	S(1)	2	90	1000	0.022
CS6	S(35)	9	90	1000	0.1
	S(10)	3	90	1000	0.033
	S(1)	1	90	1000	0.011

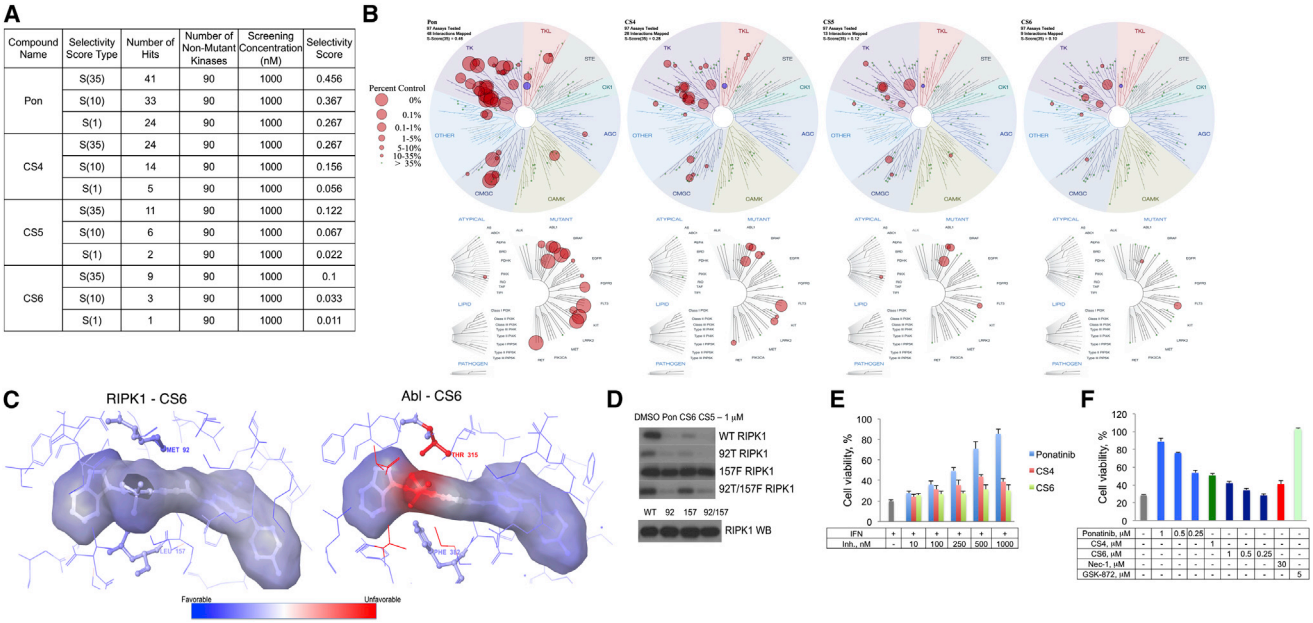

Figure 3. Selectivity Profiling of CS Analogs of Ponatinib

Inhibition of a diversity set of 97 kinases (90 WT kinase and 7 mutants, ScanEDGE, DiscoveRx) by 1 μM inhibitors.

(A) Selectivity scores of CS analogs. Selectivity score values reflect number of kinases inhibited by >65% (S35), >90% (S10), or 99% (S1).

(B) TreeView maps of kinase inhibition by ponatinib and CS analogs. Red circles indicate kinases that were inhibited by the molecules >65%. The diameter of the red circle reversely corresponds to the percentage of kinase activity remaining in the presence of inhibitor (i.e., 0% indicates complete inhibition and corresponds to the largest size of the circle). Green circles indicate kinases that were tested but were inhibited <65%. Full data are presented in Table S1.

(C) MM-GBSA energy profile analysis reveals unfavorable interactions of CS6 with Abl. Energy changes between free and bound sates of CS6 and residues in the Abl and RIPK1 binding pockets were calculated as described in the Experimental Procedures section. Colors indicate energy changes upon small molecule binding from favorable (blue) to unfavorable (red). Side chains of gatekeeper and DXG residues are shown.

(D) CS6 poorly inhibits M92T/L157F mutant of human RIPK1 kinase. FLAG-tagged kinases (amino acids 1–327) were expressed in HEK293T cells, immunoprecipitated using anti-FLAG beads, and used in 32P autophosphorylation assays with indicated concentrations of ponatinib (Pon) and CS analogs.

(E) Inhibition of IFNγ-induced cell death by Ponatinib. *RIPK1*$^{-/-}$ MEFs were treated with 10-ng/ml IFNγ in the presence of indicated concentrations of Ponatinib, CS4, and CS6 for 24 hr.

(F) Ponatinib and GSK-872 inhibit poly(I:C)-induced cell death. MEFs were treated with inhibitors, 5-μg/ml poly(I:C), and 50-μM zVAD.fmk for 24 hr. Cell viability data are presented as mean ± SD.

See also Figure S3 and Table S1.

We found that the bulky Met92 gatekeeper of RIPK1 presented a similar challenge for RIPK1 and was likely responsible for the lower observed activities of PN7, PN9, and PN13 against RIPK1 in vitro and in cells (Figure 4B) than could be expected from their high docking scores (Figure S4F). Replacing the Met92 residue of RIPK1 with a smaller Thr residue resulted in much better inhibition by these molecules, which was now on par with PN10 (Figure 4F). Since a noticeable difference in inhibition of WT and M92T RIPK1 was still seen even in the case of PN10, additional optimization of PN10 inhibitory activity through improving the fit with the Met92 residue may be possible by further changes to the linker connecting the necrostatin to the hinge binding group.

Improved Inhibition of Necrosome Formation and TNF-α Synthesis and Reduced Cytotoxicity of CS and PN Molecules

Next, we selected CS4, CS6, and PN10 for additional analyses. First, we sought to further establish the mode of action of these inhibitors by evaluating inhibition of RIPK1 and RIPK3 "necrosome" complex formation using a co-IP assay in MEF cells stimulated with TNF-α/cycloheximide/zVAD.fmk (TCZ) (Thapa et al., 2013). All ponatinib-based inhibitors efficiently blocked cell death in this system at substantially lower concentrations than those required for Nec-1 (Figures 5A and 5B) and the RIPK3 inhibitor GSK-872 (Figure S5A). Maximal protection by ponatinib itself was somewhat weaker than by CS4, CS6, and PN10 (~60% versus ~85%), likely reflecting off-target activities of ponatinib at concentrations approaching 1 μM. In agreement with a role for RIPK1 kinase activity in TCZ-driven necrosome formation (Cho et al., 2009), Nec-1 efficiently blocked necrosome assembly in TCZ-treated MEFs (Figure 5C). However, necrosome assembly was not affected by two distinct RIPK3 inhibitors, GSK-843 and GSK-872 (Kaiser et al., 2013) (Figure S5B), despite both molecules efficiently protecting cells from TCZ-induced cell death (Figure S5A; data not shown), suggesting that in TCZ-treated MEFs necrosome formation does not require the kinase activity of RIPK3. CS4, CS6, and PN10 all efficiently inhibited formation of necrosome complex at lower concentrations compared to Nec-1 (Figure 5C). Ponatinib again displayed

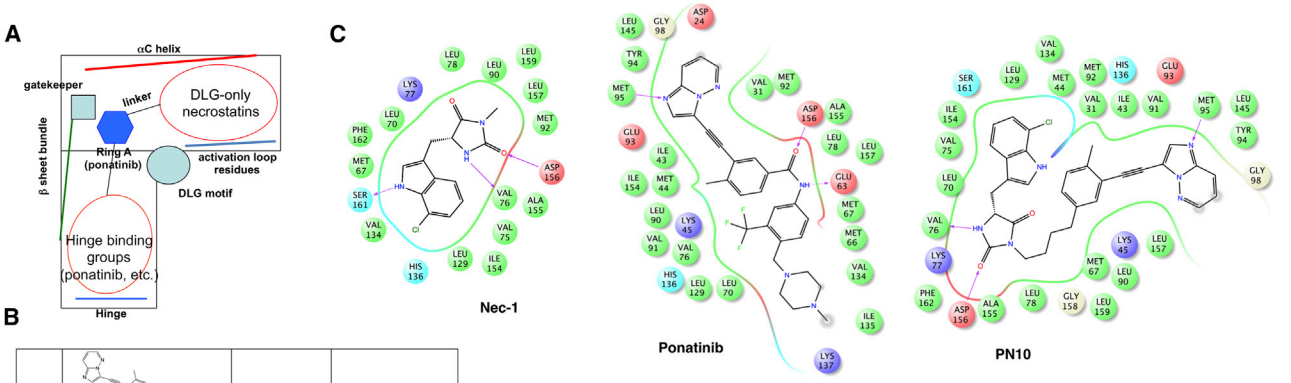

B

		IC_{50}, nM (RIPK1)	IC_{50}, nM (Necroptosis)
PN1		2633.0	332.2
PN2		1789.0	241.3
PN7		196.6	80.4
PN8		522.7	135.6
PN9		243.9	134.1
PN10		108.0	9.9
PN11		225.0	74.4
PN12		809.4	184.9
PN3		NI	1940.9
PN4		645.0	185.7
PN5		5287.0	437.5
PN6		1378.0	4382.1
PN13		1349.0	298.6

D

Compound Name	Selectivity Score Type	Number of Hits	Number of Non-Mutant Kinases	Screening Concentration (nM)	Selectivity Score
Pon	S(35)	41	90	1000	0.456
	S(10)	33	90	1000	0.367
	S(1)	24	90	1000	0.267
PN10	S(35)	2	90	1000	0.022
	S(10)	1	90	1000	0.011
	S(1)	1	90	1000	0.011

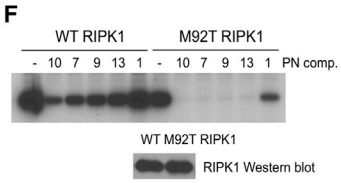

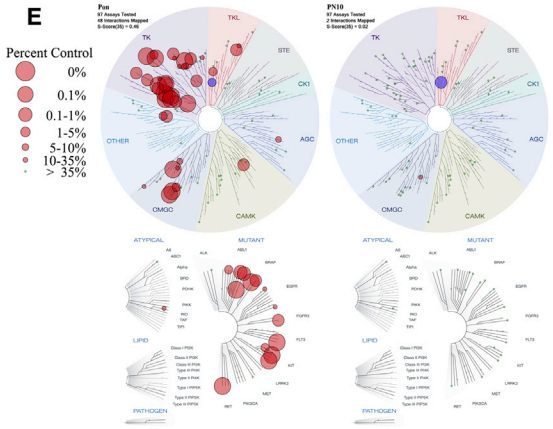

G

	Strain penalty
PN10	0
PN7	0.561
PN9	0.343/0.783
PN13	0.985
PN13/ M92T	0

Figure 4. Development of Hybrid PN RIPK1 Inhibitors

(A) General design of hybrid PN molecules, combining DLG-out Nec-1, Ring A-containing linker, and hinge-binding fragment of ponatinib.

(B) Activities of PN series of compounds. IC_{50} values against recombinant RIPK1 kinase were determined using ADPGlo assay using six-point dose range (5 μM to 20 nM) of each compound. IC_{50} values against necroptosis were determined in in TNF-treated FADD-deficient cells. Experiments were performed independently from those presented in Table 2F.

(C) Comparison of the binding poses of Nec-1 (from X-ray structure, PDB: 4ITH), ponatinib (from ponatinib/RIPK1 model; Figure 3) and PN10 (resulting from "unconstrained" Glide docking). Interaction diagrams were generated using Maestro software. PN10 forms three of four targeted hydrogen bonds to Met95 of the hinge and Val76/Asp156 in the DLG-out pocket.

(D and E) Selectivity of PN10 toward RIPK1. PN10 was screened against ScanEDGE panel (DiscoveRx) of 97 kinases at 1 μM, described in Figure 3. RIPK1 was the only kinase with >99%. Some inhibition of DYRK1b (79% inhibition) was also observed. No other kinase was inhibited >65% (other kinases in the panel indicated by green circles). Full data are presented in Table S1.

(F) PN inhibitors display increased inhibition of M92T RIPK1 mutant with Thr gatekeeper. WT and M92T mutant were expressed in 293T cells. Proteins were immunoprecipitated using anti-FLAG (M2) magnetic beads and used in ^{32}P autophosphorylation assay at 10 μM. Comparable amounts of WT and mutant kinases in kinase reactions were confirmed by western blot.

(G) Strain penalties were calculated using modified MM-GBSA algorithm for select PN hybrids based on constrained Glide docking to RIPK1. Two different binding poses were observed for PN9 with different strain values. PN10 was the only inhibitor without strain penalty. Notably, M92T mutation eliminated strain penalty in case of PN13, consistent with increased inhibition of this mutant in (F).

See also Figure S4 and Table S1.

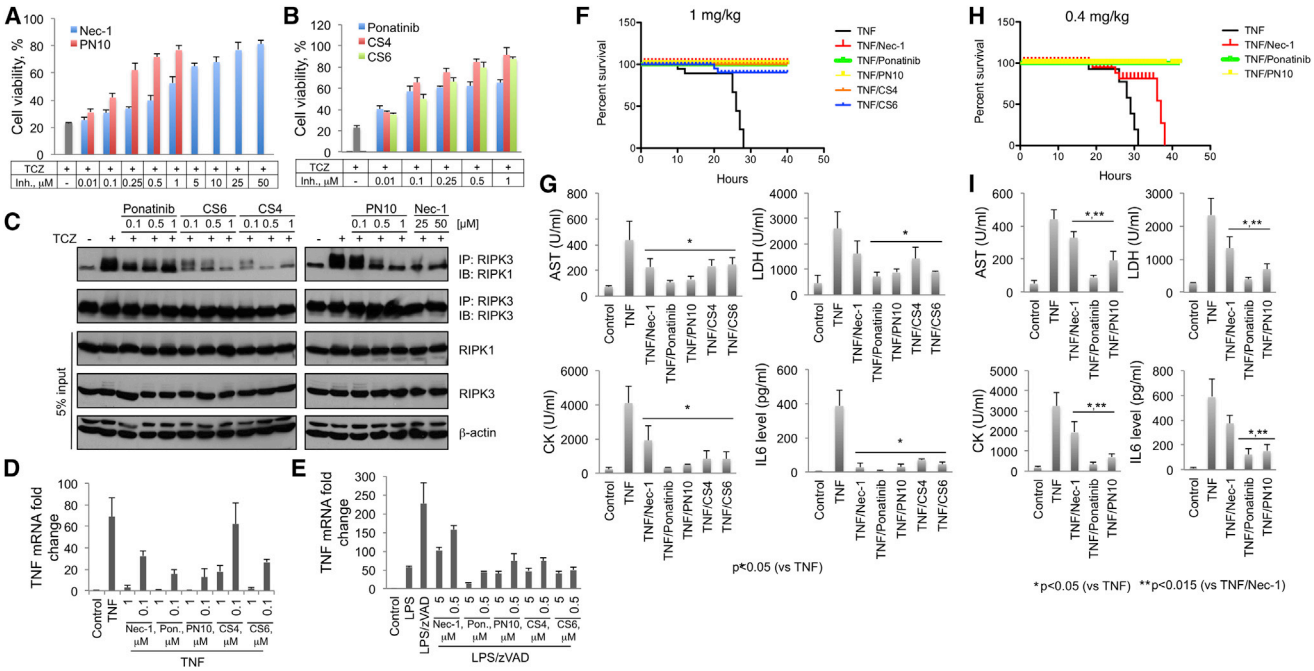

Figure 5. Inhibition of Necroptosis and Inflammation by Ponatinib Analogs

(A and B) Inhibition of TCZ-induced necroptosis in MEFs by various RIPK inhibitors. Cells were treated with 50-ng/ml mouse TNF-α, 200-ng/ml cycloheximide, and 25-μM zVAD.fmk for 18 hr in the presence of indicated concentrations of inhibitors.

(C) Ponatinib analogs inhibit necrosome formation in TCZ-stimulated MEFs. Cells were treated with 50-ng/ml mouse TNF-α, 200-ng/ml cycloheximide, and 25-μM zVAD.fmk for 6 hr in the presence of indicated concentrations of inhibitors, followed by RIPK3 immunoprecipitation.

(D and E) Ponatinib inhibits RIPK1-dependent TNFα mRNA upregulation in FADD-deficient Jurkat (D) and iBMM (E) cells. Jurkat cells were stimulated with 10-ng/ml human TNF-α for 8 hr in the presence of indicated concentrations of specific RIPK1 kinase inhibitor Nec-1, ponatinib, and indicated PN and CS analogs of ponatinib. Changes in TNF mRNA relative to GAPDH were determined by qRT-PCR. iBMM cells were stimulated with 10-ng/ml LPS and 50-μM zVAD.fmk for 7 hr.

(F and G) Ponatinib analogs block TNF-α toxicity in vivo. Survival curves are shown in (F). Reduction in TNF-induced tissue injury and inflammatory response was confirmed by assessing the circulating levels of injury markers (AST, LDH, CK) and mouse IL-6 in (G); n = 3–5 mice per group. *p < 0.05 for TNF per inhibitors versus TNF group.

(H and I) Ponatinib and PN10 display higher activity than Nec-1 in vivo. Survival curves are shown in (H). Reduction in TNF-induced tissue injury and inflammatory response was confirmed by assessing the circulating levels of injury markers (AST, LDH, CK) and mouse IL-6 in (I); n = 3–6 mice per group. *p < 0.05 for TNF/inhibitors versus TNF group, **p < 0.015 for TNF/ponatinib and TNF/PN10 groups versus TNF/Nec-1 group. Injury marker and IL6 levels data are presented as mean ± SD.

See also Figure S5.

substantial, but lower activity, consistent with weaker inhibition of cell death. Overall, these data confirmed inhibition of RIPK1-dependent necrosome formation as a cellular target of the ponatinib-based inhibitors.

Activation of cell death is not the only function of RIPK1 kinase. It has also been found to promote synthesis of TNF-α at the mRNA level independent of cell death regulation (Biton and Ashkenazi, 2011; Christofferson et al., 2012; McNamara et al., 2013). This and other cell death-independent proinflammatory activities of RIPK1 kinase are also emerging as potentially clinically relevant targets. Thus, we sought to establish whether the activity of ponatinib-based inhibitors extends beyond cell death regulation by RIPK1. TNF-α stimulation of Jurkat cells and LPS/zVAD.fmk stimulation of immortalized macrophages led to robust increase in TNF-α mRNA, inhibited by Nec-1. Ponatinib, CS4, CS6, and PN10 again efficiently inhibited this cell death-independent function of RIPK1 kinase (Figures 5D and 5E), revealing potentially important anti-inflammatory properties of ponatinib and its RIPK1-selective derivatives.

Finally, ponatinib displayed significant cytotoxicity at concentrations >1 μM (Figures S5C–S5E). We found that the increased kinase selectivity of CS molecules and PN10 also translated into substantially lower cytotoxicity (Figures S5C–S5E), improving one of the significant limitations of ponatinib as a cytoprotective and anti-inflammatory agent.

Inhibition of In Vivo TNF-α Toxicity by Ponatinib Analogs

To evaluate the potential therapeutic efficacy of ponatinib-based inhibitors, we examined their ability to counteract toxicity of TNF-α in vivo, which was previously shown to reflect activation of necroptotic RIPK1 and RIPK3 signaling (Duprez et al., 2011). Intraperitoneal injection of Nec-1 at 1-mg/kg dose provided significant protection from injury and reduced circulating levels of interleukin-6 (IL-6) and prevented death of the animals, consistent with previous reports (Duprez et al., 2011; Takahashi et al., 2012). Ponatinib completely prevented toxicity of TNF-α, revealing for the first time the unexpected cytoprotective properties of this anti-cancer agent in vivo (Figures 5F and 5G). PN10,

CS4, and CS6 were also fully protective at the 1-mg/kg dose (Figures 5F and 5G). At lower 0.4-mg/kg dose, both ponatinib and PN10 displayed significantly higher activity than Nec-1 with respect to survival and injury markers (Figures 5H and 5I). The improved activity of PN10 over Nec-1 demonstrated that our guided approach has indeed led to the development of significantly improved selective in vivo inhibitor of RIPK1-dependent cell death and inflammation.

DISCUSSION

RIPK1 and RIPK3 first emerged as acting in concert in activating necroptosis (Cho et al., 2009). However, more recent genetic and pharmacologic evidence demonstrated that these two proteins may possess multiple nonoverlapping functions in the regulation of inflammation (Cuda et al., 2014; Lukens et al., 2013), apoptosis (Dondelinger et al., 2013), and necroptosis (Dannappel et al., 2014; Dillon et al., 2014; Kaiser et al., 2014; Orozco et al., 2014). This array of functions has inspired us and others to pursue development of RIPK1 (Degterev et al., 2008; Harris et al., 2013) and RIPK3 (Kaiser et al., 2013) inhibitors. Our current finding that ponatinib dually targets RIPK1 and RIPK3 represents a unique and important property of this molecule, making it a useful tool compound to further evaluate therapeutic consequences of inhibiting pathologic RIPK signaling, where multiple mechanisms of RIPK1- and RIPK3-dependent cell death may be activated simultaneously in different cell populations, depending on the specifics of their state or individual regulation. The lack of selectivity and reported safety concerns (http://www.fda.gov/safety/medwatch/safetyinformation/safetyalertsforhumanmedicalproducts/ucm370971.htm) may exclude broad use of ponatinib as a cytoprotective and anti-inflammatory agent. However, cancer-associated inflammation could be one specific area where the ability of ponatinib to block RIPK1 and RIPK3 could be of immediate value. Inflammatory mediators, including cytokines, microbial PAMPSs/DAMPs, and carcinogenic agents such as asbestos fibers, promote tumorigenesis by contributing to an inflammatory microenvironment in certain human cancers (Elinav et al., 2013). As many of these proinflammatory agents have also been shown to activate RIPK1 and RIPK3 kinases (Vanlangenakker et al., 2012), ponatinib may help reveal functions for RIPKs in cancer-associated inflammatory signaling and facilitate translation of these results into clinical benefits.

The discovery of RIPK1 and RIPK3 activity of ponatinib prompted us to expand its SAR via two different approaches to achieve RIPK1 selective inhibitors. Our studies with the CS series revealed an unexpected induced fit mechanism for inhibition of RIPK1. We found that increasing the size of the phenyl ring (Ring A) substituent of ponatinib from *i*-propyl to *t*- or *c*-butyl led to an abrupt "activity cliff" resulting in selective inhibition of RIPK1 compared with other RIPKs and Abl (Tables 2 and S1). While statically RIPK1 contains a more restricted Ring A pocket as demonstrated by poor activity of ponatinib and CS molecules against L157F mutant of RIPK1 (Figure 3D), this paradox can be explained by the greater plasticity or RIPK1 due to the presence of less bulky and more conformationally flexible DLG motif that allows RIPK1 (but not DFG kinases Abl, RIPK2 or RIPK3) to accommodate the bulkier Ring A through induced fit. Additional specific differences in the packing of the activation loop and geometry of the Ring A pocket likely further differentiate affinities of ponatinib analogs toward RIPK2 and RIPK3 versus Abl as we have observed that these kinases, unlike Abl are poorly inhibited even by the isopropyl CS4 analog. Overall our data reveal a possible direction for increasing selectivity of type 2 inhibitors by taking advantage of the differential flexibility of DXG pockets. Strikingly, only 4 of 44 (9%) DFG-motif containing ponatinib-inhibited kinase targets were efficiently inhibited by CS6 (>65% at 1 μM), while this was the case for three of four (75%) non-DFG kinases (Table S2). Thus, our findings may be particularly applicable for targeting non-DFG kinases.

While small changes to the ponatinib scaffold represent one direction for achieving additional activities for ponatinib-like molecules, we show that a fragment approach combining Nec-1 with the ATP pocket-binding moiety of ponatinib (e.g., PN10) led to a much greater improvement in selectivity and cellular activity compared with both Nec-1 and ponatinib (Table 2). Several conclusions can be made based on the SAR of the PN series. First, despite ponatinib (and other type 2 inhibitors) binding to Glu-in/DXG-out kinase conformations, dictated by interactions of its central amide group with a Glu residue in the αC helix (Liu and Gray, 2006; Zhou et al., 2011, Zhao et al., 2014), its hinge binding fragment appears to be compatible with the Glu-out/DLG-out conformation of RIPK1 required for Nec-1 binding (Xie et al., 2013). It is unlikely that PN10 binds to the Glu-in/DLG-out conformation, as this would be expected to cause a steric clash between the Met67 residue in the αC helix of RIPK1 and the hydantoin of Nec-1 (Figure S4B). Second, we found that multiple PN analogs, selected using constrained GLIDE XP docking, underperformed due to clashes with the Met92 gatekeeper (Figure 4F). Furthermore, we calculated strain penalties for PN analogs using a modified MM-GBSA algorithm to understand how PN series activities can be predicted computationally. This calculation provides a cumulative index of various strains occurring in the ligand upon constrained docking to the target. We observed that PN10 was the only analog lacking strain, consistent with its highest affinity (Figure 4G). Furthermore, strain of the less active analog PN13 was eliminated in the M92T mutant of RIPK1, consistent with comparable inhibition of this mutant by PN10 and PN13 (Figure 4F). Overall, our data suggest that structural data available for RIPK1 in combination with GLIDE XP docking and strain analysis are sufficient for predicting RIPK1 binding properties by hybrid molecules with a high degree of fidelity. Finally, previous data showed that Nec-1 is a uniquely selective kinase inhibitor (Christofferson et al., 2012), and changes to most positions of this molecule lead to the loss of activity (Teng et al., 2005), limiting options for further optimization. Our data identify the direction for improving Nec-1 activity without sacrificing specificity. The development of PN10 captured most of ponatinib's activity in vivo, but also provided much improved kinase selectivity, characteristic for Nec-1. High cellular activity of PN10, its selectivity toward RIPK1, and potent inhibition of TNF-α toxicity in vivo warrant further evaluation of the therapeutic potential of this molecule in other preclinical models of human pathology, where the contribution of RIPK1 has been already established

(Linkermann and Green, 2014). Our data with M92T RIPK1 also indicate that steric hindrance with the Met92 gatekeeper still exists for PN10, suggesting that further improvement of this molecule may be possible through finding a better fit between the gatekeeper and Ring A of PN10. In conclusion, we wish to highlight the potential broad applicability of this design approach to other kinases targeted by ponatinib, with the goal of obtaining ''hybrids'' retaining PN10's binding mode, but containing modifications to the necrostatin moiety to fit the DXG pockets of these other kinases.

EXPERIMENTAL PROCEDURES

Reagents and Chemicals

All of the reagents and chemicals were purchased from Sigma, Fisher, or VWR unless otherwise stated. RIPK1, actin, and tubulin antibodies were purchased from Cell Signaling Technologies; RIPK3 antibody was from ProSci.

Cell Lines

FADD-deficient Jurkat cells and HEK293T cells were purchased from ATCC. HEKBlue cells were purchased from Invitrogen. Immortalized bone marrow-derived macrophages (iBMM) were a gift of Dr. Kate Fitzgerald (UMass Medical Center). Cells were maintained in RPMI (Invitrogen, Jurkat cells) or DMEM (Fisher) supplemented with 10% fetal bovine serum (FBS; Sigma-Aldrich) and 1% antibiotic-antimycotic mix (Invitrogen). *RIPK1*$^{+/+}$ and *RIPK1*$^{-/-}$ MEFs were a kind gift of Drs. William Kaiser and Ed Mocarski (Emory University). MEFs were cultured in DMEM supplemented with 10% FBS (Hyclone) and 1% antibiotic-antimycotic mix.

Animals

All animal experiments were performed with approval of the Institutional Animal Care and Use Committee of Tufts University and Fox Chase Cancer Center. Female C57BL6/J mice (6–8 weeks old) were purchased from approved vendor (Charles River Laboratories). Animals were housed in cages with a light/dark cycle. All efforts were made to minimize the numbers of animals and their suffering.

TNF-Induced Injury

To study the effect of the compounds in TNF-induced injury in mouse model, female C57BL6/J mice were injected intraperitoneally with 100 μl of vehicle (25% PEG400 in PBS) or the compounds (Nec-1, ponatinib, PN10, CS4, and CS6, formulated in the above vehicle) at the doses of 1 and 0.4 mg/kg. At 15 min later, animals were injected intravenously through the tail vein with either 5 μg per mouse of recombinant mouse TNF-α (Cell Guidance System) or sterile PBS in a volume of 100 μl. Blood samples were collected 30 hr after injection or earlier if moribund through submandibular bleed. Serum samples were submitted to IDEXX laboratories for analysis of aspartate aminotransferase (AST), creatine kinase (CK), and lactate dehydrogenase (LDH) levels. IL-6 ELISA was performed using 25 μl of serum using mouse IL-6 ELISA kit (Meso Scale Discovery). Statistical analysis was performed using Student's t test (GraphPad Prism 5).

SUPPLEMENTAL INFORMATION

Supplemental Information includes Supplemental Experimental Procedures, five figures, and two tables and can be found with this article online at http://dx.doi.org/10.1016/j.celrep.2015.02.052.

AUTHOR CONTRIBUTIONS

M.N., R.J.T., S.N., and D.S. performed cell-based experiments. J.L.M., S.S., and A.D. performed in vitro kinase assays. S.S.R. performed and interpreted computational modeling studies. C.S. synthesized and characterized small molecule inhibitors. M.N. performed in vivo experiments. S.S.R, S.B., G.D.C., and A.D. designed, analyzed, and interpreted experiments. M.N., C.S., S.S.R., P.J.G., J.B., J.Y., S.B., G.D.C., and A.D. wrote and revised the manuscript.

ACKNOWLEDGMENTS

This work was supported in part by grants from the NIH to A.D. (R01 GM080356, R01 GM084205) and S.B. (R01 CA168621 and R21 AI113469) and the Chemical Biology Interdisciplinary Program at the University of Houston to C.S. We thank Dr. Alex Bullock (Oxford University) for providing recombinant RIPK2 kinase, Dr. Kate Fitzgerald (University of Massachusetts School of Medicine) and Drs. William Kaiser and Edward Mocarski (Emory University) for *RIPK1*$^{+/+}$ and *RIPK1*$^{-/-}$ cells, Drs. Hairong Hou and Jiong Chen (Sundia Meditech) for help synthesizing PN compounds, and Dr. You-Jun Fu (University of Connecticut) for performing high-resolution mass spectrometry (HRMS) analysis. P.J.G. and J.B. are employees of GlaxoSmithKline. J.Y., G.D.C., and A.D. are scientific co-founders of Incro Pharmaceuticals, a biotechnology start-up company focused on the development of necroptosis inhibitors.

Received: November 5, 2014
Revised: January 13, 2015
Accepted: February 23, 2015
Published: March 19, 2015

REFERENCES

Beard, H., Cholleti, A., Pearlman, D., Sherman, W., and Loving, K.A. (2013). Applying physics-based scoring to calculate free energies of binding for single amino acid mutations in protein-protein complexes. PLoS ONE *8*, e82849.

Biton, S., and Ashkenazi, A. (2011). NEMO and RIP1 control cell fate in response to extensive DNA damage via TNF-α feedforward signaling. Cell *145*, 92–103.

Cho, Y.S., Challa, S., Moquin, D., Genga, R., Ray, T.D., Guildford, M., and Chan, F.K. (2009). Phosphorylation-driven assembly of the RIP1-RIP3 complex regulates programmed necrosis and virus-induced inflammation. Cell *137*, 1112–1123.

Choi, S., Keys, H., Staples, R.J., Yuan, J., Degterev, A., and Cuny, G.D. (2012). Optimization of tricyclic Nec-3 necroptosis inhibitors for in vitro liver microsomal stability. Bioorg. Med. Chem. Lett. *22*, 5685–5688.

Christofferson, D.E., and Yuan, J. (2010). Necroptosis as an alternative form of programmed cell death. Curr. Opin. Cell Biol. *22*, 263–268.

Christofferson, D.E., Li, Y., Hitomi, J., Zhou, W., Upperman, C., Zhu, H., Gerber, S.A., Gygi, S., and Yuan, J. (2012). A novel role for RIP1 kinase in mediating TNFα production. Cell Death Dis. *3*, e320.

Cuda, C.M., Misharin, A.V., Gierut, A.K., Saber, R., Haines, G.K., 3rd, Hutcheson, J., Hedrick, S.M., Mohan, C., Budinger, G.S., Stehlik, C., and Perlman, H. (2014). Caspase-8 acts as a molecular rheostat to limit RIPK1- and MyD88-mediated dendritic cell activation. J. Immunol. *192*, 5548–5560.

Dannappel, M., Vlantis, K., Kumari, S., Polykratis, A., Kim, C., Wachsmuth, L., Eftychi, C., Lin, J., Corona, T., Hermance, N., et al. (2014). RIPK1 maintains epithelial homeostasis by inhibiting apoptosis and necroptosis. Nature *513*, 90–94.

Degterev, A., Huang, Z., Boyce, M., Li, Y., Jagtap, P., Mizushima, N., Cuny, G.D., Mitchison, T.J., Moskowitz, M.A., and Yuan, J. (2005). Chemical inhibitor of nonapoptotic cell death with therapeutic potential for ischemic brain injury. Nat. Chem. Biol. *1*, 112–119.

Degterev, A., Hitomi, J., Germscheid, M., Ch'en, I.L., Korkina, O., Teng, X., Abbott, D., Cuny, G.D., Yuan, C., Wagner, G., et al. (2008). Identification of RIP1 kinase as a specific cellular target of necrostatins. Nat. Chem. Biol. *4*, 313–321.

Dillon, C.P., Weinlich, R., Rodriguez, D.A., Cripps, J.G., Quarato, G., Gurung, P., Verbist, K.C., Brewer, T.L., Llambi, F., Gong, Y.N., et al. (2014). RIPK1 blocks early postnatal lethality mediated by caspase-8 and RIPK3. Cell *157*, 1189–1202.

Dondelinger, Y., Aguileta, M.A., Goossens, V., Dubuisson, C., Grootjans, S., Dejardin, E., Vandenabeele, P., and Bertrand, M.J. (2013). RIPK3 contributes

to TNFR1-mediated RIPK1 kinase-dependent apoptosis in conditions of cIAP1/2 depletion or TAK1 kinase inhibition. Cell Death Differ. *20*, 1381–1392.

Duprez, L., Takahashi, N., Van Hauwermeiren, F., Vandendriessche, B., Goossens, V., Vanden Berghe, T., Declercq, W., Libert, C., Cauwels, A., and Vandenabeele, P. (2011). RIP kinase-dependent necrosis drives lethal systemic inflammatory response syndrome. Immunity *35*, 908–918.

Elinav, E., Nowarski, R., Thaiss, C.A., Hu, B., Jin, C., and Flavell, R.A. (2013). Inflammation-induced cancer: crosstalk between tumours, immune cells and microorganisms. Nat. Rev. Cancer *13*, 759–771.

Friesner, R.A., Banks, J.L., Murphy, R.B., Halgren, T.A., Klicic, J.J., Mainz, D.T., Repasky, M.P., Knoll, E.H., Shelley, M., Perry, J.K., et al. (2004). Glide: a new approach for rapid, accurate docking and scoring. 1. Method and assessment of docking accuracy. J. Med. Chem. *47*, 1739–1749.

Harris, P.A., Bandyopadhyay, D., Berger, S.B., Campobasso, N., Capriotti, C.A., Cox, J.A., Dare, L., Finger, J.N., Hoffman, S.J., Kahler, K.M., et al. (2013). Discovery of Small Molecule RIP1 Kinase Inhibitors for the Treatment of Pathologies Associated with Necroptosis. ACS Med. Chem. Lett. *4*, 1238–1243.

Hayes, J.M., Skamnaki, V.T., Archontis, G., Lamprakis, C., Sarrou, J., Bischler, N., Skaltsounis, A.L., Zographos, S.E., and Oikonomakos, N.G. (2011). Kinetics, in silico docking, molecular dynamics, and MM-GBSA binding studies on prototype indirubins, KT5720, and staurosporine as phosphorylase kinase ATP-binding site inhibitors: the role of water molecules examined. Proteins *79*, 703–719.

He, S., Liang, Y., Shao, F., and Wang, X. (2011). Toll-like receptors activate programmed necrosis in macrophages through a receptor-interacting kinase-3-mediated pathway. Proc. Natl. Acad. Sci. USA *108*, 20054–20059.

Huron, D.R., Gorre, M.E., Kraker, A.J., Sawyers, C.L., Rosen, N., and Moasser, M.M. (2003). A novel pyridopyrimidine inhibitor of abl kinase is a picomolar inhibitor of Bcr-abl-driven K562 cells and is effective against STI571-resistant Bcr-abl mutants. Clin. Cancer Res. *9*, 1267–1273.

Jagtap, P.G., Degterev, A., Choi, S., Keys, H., Yuan, J., and Cuny, G.D. (2007). Structure-activity relationship study of tricyclic necroptosis inhibitors. J. Med. Chem. *50*, 1886–1895.

Kaiser, W.J., Sridharan, H., Huang, C., Mandal, P., Upton, J.W., Gough, P.J., Sehon, C.A., Marquis, R.W., Bertin, J., and Mocarski, E.S. (2013). Toll-like receptor 3-mediated necrosis via TRIF, RIP3, and MLKL. J. Biol. Chem. *288*, 31268–31279.

Kaiser, W.J., Daley-Bauer, L.P., Thapa, R.J., Mandal, P., Berger, S.B., Huang, C., Sundararajan, A., Guo, H., Roback, L., Speck, S.H., et al. (2014). RIP1 suppresses innate immune necrotic as well as apoptotic cell death during mammalian parturition. Proc. Natl. Acad. Sci. USA *111*, 7753–7758.

Levinson, N.M., Kuchment, O., Shen, K., Young, M.A., Koldobskiy, M., Karplus, M., Cole, P.A., and Kuriyan, J. (2006). A Src-like inactive conformation in the abl tyrosine kinase domain. PLoS Biol. *4*, e144.

Linkermann, A., and Green, D.R. (2014). Necroptosis. N. Engl. J. Med. *370*, 455–465.

Liu, Y., and Gray, N.S. (2006). Rational design of inhibitors that bind to inactive kinase conformations. Nat. Chem. Biol. *2*, 358–364.

Lukens, J.R., Vogel, P., Johnson, G.R., Kelliher, M.A., Iwakura, Y., Lamkanfi, M., and Kanneganti, T.D. (2013). RIP1-driven autoinflammation targets IL-1α independently of inflammasomes and RIP3. Nature *498*, 224–227.

Maki, J.L., and Degterev, A. (2013). Activity assays for receptor-interacting protein kinase 1:a key regulator of necroptosis. Methods Mol. Biol. *1004*, 31–42.

Maki, J.L., Tres Brazell, J., Teng, X., Cuny, G.D., and Degterev, A. (2013). Expression and purification of active receptor interacting protein 1 kinase using a baculovirus system. Protein Expr. Purif. *89*, 156–161.

McNamara, C.R., Ahuja, R., Osafo-Addo, A.D., Barrows, D., Kettenbach, A., Skidan, I., Teng, X., Cuny, G.D., Gerber, S., and Degterev, A. (2013). Akt Regulates TNFα synthesis downstream of RIP1 kinase activation during necroptosis. PLoS ONE *8*, e56576.

Orozco, S., Yatim, N., Werner, M.R., Tran, H., Gunja, S.Y., Tait, S.W., Albert, M.L., Green, D.R., and Oberst, A. (2014). RIPK1 both positively and negatively regulates RIPK3 oligomerization and necroptosis. Cell Death Differ. *21*, 1511–1521.

Takahashi, N., Duprez, L., Grootjans, S., Cauwels, A., Nerinckx, W., DuHadaway, J.B., Goossens, V., Roelandt, R., Van Hauwermeiren, F., Libert, C., et al. (2012). Necrostatin-1 analogues: critical issues on the specificity, activity and in vivo use in experimental disease models. Cell Death Dis. *3*, e437.

Teng, X., Degterev, A., Jagtap, P., Xing, X., Choi, S., Denu, R., Yuan, J., and Cuny, G.D. (2005). Structure-activity relationship study of novel necroptosis inhibitors. Bioorg. Med. Chem. Lett. *15*, 5039–5044.

Teng, X., Keys, H., Jeevanandam, A., Porco, J.A., Jr., Degterev, A., Yuan, J., and Cuny, G.D. (2007). Structure-activity relationship study of [1,2,3]thiadiazole necroptosis inhibitors. Bioorg. Med. Chem. Lett. *17*, 6836–6840.

Teng, X., Keys, H., Yuan, J., Degterev, A., and Cuny, G.D. (2008). Structure-activity relationship and liver microsome stability studies of pyrrole necroptosis inhibitors. Bioorg. Med. Chem. Lett. *18*, 3219–3223.

Thapa, R.J., Nogusa, S., Chen, P., Maki, J.L., Lerro, A., Andrake, M., Rall, G.F., Degterev, A., and Balachandran, S. (2013). Interferon-induced RIP1/RIP3-mediated necrosis requires PKR and is licensed by FADD and caspases. Proc. Natl. Acad. Sci. USA *110*, E3109–E3118.

Upton, J.W., Kaiser, W.J., and Mocarski, E.S. (2012). DAI/ZBP1/DLM-1 complexes with RIP3 to mediate virus-induced programmed necrosis that is targeted by murine cytomegalovirus vIRA. Cell Host Microbe *11*, 290–297.

Vanlangenakker, N., Vanden Berghe, T., and Vandenabeele, P. (2012). Many stimuli pull the necrotic trigger, an overview. Cell Death Differ. *19*, 75–86.

Xie, T., Peng, W., Liu, Y., Yan, C., Maki, J., Degterev, A., Yuan, J., and Shi, Y. (2013). Structural basis of RIP1 inhibition by necrostatins. Structure *21*, 493–499.

Zhao, Z., Wu, H., Wang, L., Liu, Y., Knapp, S., Liu, Q., and Gray, N.S. (2014). Exploration of type II binding mode: A privileged approach for kinase inhibitor focused drug discovery? ACS Chem. Biol. *9*, 1230–1241.

Zhou, T., Commodore, L., Huang, W.S., Wang, Y., Thomas, M., Keats, J., Xu, Q., Rivera, V.M., Shakespeare, W.C., Clackson, T., et al. (2011). Structural mechanism of the Pan-BCR-ABL inhibitor ponatinib (AP24534): lessons for overcoming kinase inhibitor resistance. Chem. Biol. Drug Des. *77*, 1–11.